Journal of the Brazilian Society of Mechanical Sciences and Engineering (2021) 43:570
https://doi.org/10.1007/s40430-021-03297-7

TECHNICAL PAPER

Structure-acoustic simulation using the modal expansion method and the optimum sensor placement

B. K. Jung[1] · J. R. Cho[2]

Received: 7 May 2020 / Accepted: 17 November 2021 / Published online: 29 November 2021

Abstract
This paper is concerned with the application of the modal expansion method (MEM) to the vibro-acoustic simulation of flexible vibrating structures. The structural vibration field due to the external excitation is expanded by a FEM-based modal expansion method, and the corresponding normal velocity is transferred into the acoustic FE mesh that is generated for the acoustic analysis. In this kind of acoustic simulation, the numerical results are definitely influenced by the accuracy of the expanded vibration field using the modal expansion method, which is in turn influenced by the sensor placement for extracting and determining the reduced numerical mode shapes and the modal participation factors that are essential for the modal expansion method. In this context, the investigation of its effect on the numerical accuracy of the acoustic analysis is of importance. We in this paper compare the acoustic analysis results, such as the sound patterns, power, and pressures, between the regular and optimum sensor placements with MSC/Nastran results for three different boundary conditions.

Keywords Structural vibration · Acoustic sound · Modal expansion · Optimum sensor placement · Acoustic analysis · Acoustical pattern · Acoustic power and pressure

1 Introduction

The reduction of noise has been a continuing subject in a whole range of fields, and it becomes more crucial as the environmental-friendly policy is being rapidly intensified worldwide [1]. For example, traffic noise of automotive and railway vehicles, indoor noise of home appliances, radiation noise of aircraft and submarine, and various industrial noises would be the major concerns. This situation naturally made the noise level one of the most important performances in all the engineering applications, which emphasized the importance of the prediction and evaluation of noise level in the process of product development [2]. The noise level of products was traditionally evaluated by means of experimental tools at the prototype stage, but the advances in computer modeling and simulation technologies made its prediction possible even at the stage of concept design [3]. There exist many kinds of noise sources and their transmission is also diverse, but the most of noises around us are attributed to structural-acoustic radiation [4].

The interaction between the structural vibration and the surrounding air pressure induces acoustic wave propagation in the air. In the strict sense, structural acoustic radiation is an intrinsically coupled problem between the structural vibration field and the acoustic pressure field [5, 6]. When such an interaction between two fields is fully considered, the numerical analysis of the structural–acoustic problem requires either the elaborate derivation of a two-field monolithic formulation [7] or the staggered iterative solving scheme [8, 9]. However, both the complexity and difficulty in the numerical formulation and simulation could be greatly relaxed when the effect of acoustic pressure on the structural vibration is not significant. In fact, in the structure-acoustic system, the effect of acoustic pressure on the dynamic structural deformation becomes negligible when the structural stiffness is much higher than the acoustic impedance.

In such cases, the structural-acoustic problem can be separately and indirectly solved, by taking the normal velocity data of the structure which can also be separately

Technical Editor: José Roberto de França Arruda.

✉ J. R. Cho
jrcho@hongik.ac.kr

[1] Agency for Defense Development, Jinhae Gu, Changwon City 51678, Kyoungnam, Korea

[2] Department of Naval Architecture and Ocean Engineering, Hongik University, Sejong 30016, Korea

obtained by the structural vibration analysis as the boundary condition for the acoustic simulation [10]. In general, the normal velocity data on the outer structure surface which is interfaced with the surrounding air are extracted using the finite element vibration analysis. But, those can also be obtained by the modal expansion method (MEM) [11] that is widely used to reproduce and visualize the vibration field of structure using the measured modal parameters. In this method, the dynamic displacement field of the vibrating structure is reproduced in terms of the reduced number of natural modes and their modal participation factors that are measured and determined using a number of vibration sensors. However, the quality of the reproduced vibration field is influenced by the sensor positions [12–14] as well as the number of vibration sensors, which in turn affects the numerical accuracy of structural-acoustic analysis.

In this context, the purpose of the current study is to present the numerical analysis procedure for the structure-acoustic problem by utilizing the modal expansion method and to investigate the influence of sensor position on numerical accuracy. The reduced natural modes are extracted from the numerical natural modes that are obtained by the FE modal analysis for the illustrative purpose, and the modal participation factors are determined using the measured vibration data. To extract and determine these modal parameters, the regular (i.e., uniform) and optimum sensor placements are used. The optimum sensor positions are determined by utilizing a genetic algorithm [15, 16], and the acoustic analysis is carried out by the acoustic transfer vector (ATV) technique in LMS Virtual. Lab [17] using the reproduced vibration data. The proposed method is illustrated through the numerical experiment with cylindrical shell-like structures. And, the vibro-acoustic results between the regular and optimum sensor placements are compared with MSC/Nastran results for three different boundary conditions: clamped-free, free-free, and clamped–clamped.

2 Acoustical boundary value problem

Referring to Fig. 1, let us consider a 3-D acoustical problem in which the structural vibratory energy is radiating through an infinite air domain. The vibrating body B is a thin elastic shell-like structure of thickness t, diameter D and length L. The dynamic displacement field $u(x;t)$ of body is interacted with the acoustic velocity field $V(x;t)$ of air at their common interface such that $V \cdot n = -\dot{u} \cdot n$ [18, 19]. For the purpose of computation, an infinite air medium enclosing the vibrating structure is truncated to a finite spherical domain $\Omega \in \Re^3$ with the radius R_X, and the Cartesian coordinate system with its origin designated at the center of structure is adopted. Then, the time-harmonic acoustic pressure field $p(x;t) = p(x) \cdot e^{i\omega t}$ within the air domain Ω that is induced by the structural vibration is governed by the Helmholtz equation, which is defined by

$$\Delta p + \kappa^2 p = 0 \quad \text{in} \quad \Omega \tag{1}$$

and the Neumann boundary condition given by

$$V_n = V_n^0 \quad \text{on} \quad S_N \tag{2}$$

and the radiation condition:

$$i\kappa p + \frac{\partial p}{\partial r} = O\left(X^{-(d-1)/2}\right) \quad \text{on} \quad \Gamma_X \tag{3}$$

with $\kappa = \omega/c$ and $V_n = V \cdot n$ being the wavenumber and the normal flow velocity. In which, $d(=3)$ is the spatial dimension of the problem, and ω and c the angular frequency and the speed of sound, respectively. In the limit $R_X \to \infty$, the domain becomes unbounded and the radiation condition (3) enforced on the truncated artificial boundary Γ_X becomes the Sommerfeld condition [20].

The weak form of the acoustical boundary value problem given in Eqs. (1)–(3) can be derived according to the variational formulation. Introducing test function q and

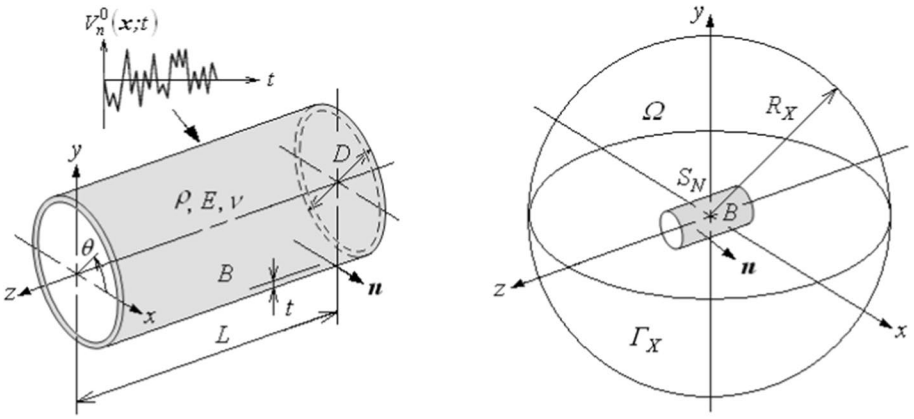

Fig. 1 Acoustical boundary value problem for a flexible vibrating structure

employing Green's theorem leads to: Find the acoustic pressure $p(x;t)$ such that

$$\int_{\Omega}\left(\nabla p\cdot\nabla q-\kappa^2 pq\right)dv=\int_{S_N} i\rho\omega V_n^0 ds - \int_{\Gamma_X}\left(i\kappa p-O\left(X^{-(d-1)/2}\right)\right)q\,ds=0 \tag{4}$$

for every admissible pressure field $q(x;t)$. Here, ρ indicates the air density, and the Euler equation $\nabla p=-\rho V$ is employed for the derivation of the first term on the right-hand side (RHS). The numerical implementation of this weak form can be done by various methods, among which the finite element method, the combined finite/infinite element method, and the boundary element method (BEM) are widely employed [21, 22]. In case of the finite element-based approach, the second term on the RHS can be dropped out when the test and trial functions are defined so as to satisfy the radiation condition (3) [10]. Meanwhile, the wave reflection phenomenon at the truncated artificial boundary Γ_X can be suppressed by employing the special non-reflecting boundary condition [23].

In the current study, the above boundary value problem is basically solved by the finite element method, but the normal flow velocity V_n^0 in Eq. (4) (more exactly, the normal structural velocity $\dot{u}_n^0$), a source of radiation noise, is indirectly calculated by the FEM-based modal expansion method and transferred into the acoustic FE mesh. As will be addressed in detail in the next section, the structural vibration field $u(x;t)$ is expanded in terms of the mode shapes and the modal participation factors that are obtained by the finite element modal/vibration analyses.

3 Modal expansion of the vibration field

The vibration field $u(x;t)$ of a structure subject to the external excitation $f(t)$ can be expressed as a linear combination of natural modes Φ_I such that $u(x;t)=\Phi_1(x)q_1(t)+\Phi_2(x)q_2+\cdots$, with $q_I(t)$ being the modal participation factors. Based on this fact, the modal expansion method (MEM) is used to approximate (i.e., reproduce) the vibration field with the total of n lowest natural modes. In terms of using the limited number of natural modes, the natural modes selected for the modal expansion are called by the reduced natural modes $\Phi_I^r(I=1,\,2,\ldots,n)$. The reduced natural modes can be experimentally measured using the total of N vibration sensors, as shown in Fig. 2a, or by extracting from the numerical natural modes $\Phi_I=\left\{\phi_I^1,\phi_I^2,\cdots,\phi_I^m\right\}^T$ which were obtained by the FE modal analysis using an m-DOF mesh. In case of the numerical extraction, the finite element mesh for the modal analysis is generated such that m is sufficiently larger than n. And, each numerically reduced natural mode $\Phi_I^r=\left\{\phi_I^1,\phi_I^2,\cdots,\phi_I^N\right\}^T$ having N components is extracted from the numerical natural mode Φ_I by taking only the components corresponding to the finite element nodes where the vibration sensors are positioned.

Regardless of how those are obtained, a common prominent feature of the reduced natural modes is the disobedience of the orthogonality between themselves. It is natural because those are not obtained through the mathematically orthogonal extraction process such as Jacobi iteration. Such disobedience is usually evaluated by the modal assurance criterion (MAC) [24] which is defined by

$$\mathrm{MAC}_{IJ}=\mathrm{MAC}\left(\Phi_I^{r,T}\Phi_J^r\right)=\left|\Phi_I^{r,T}\Phi_J^r\right|^2/\left(\Phi_I^{r,T}\Phi_I^r\right)\left(\Phi_J^{r,T}\Phi_J^r\right) \tag{5}$$

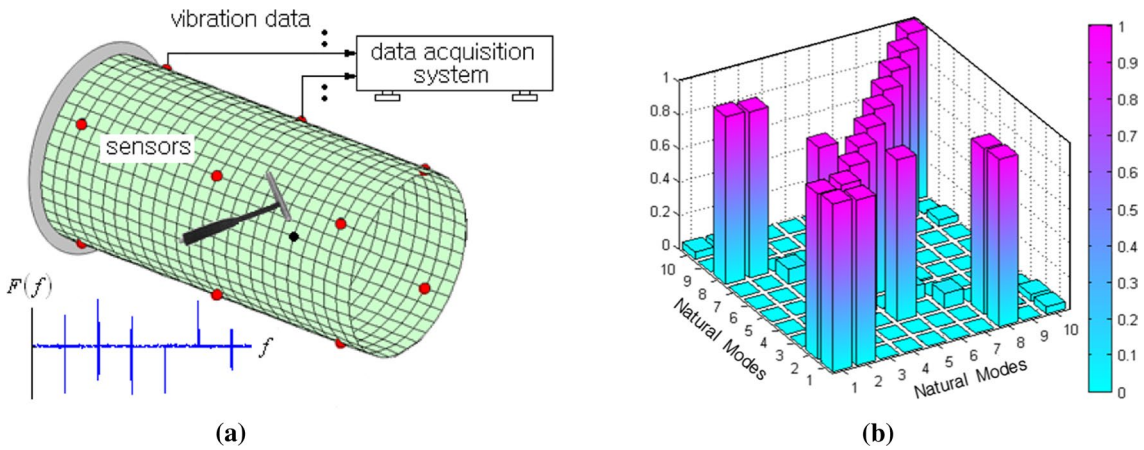

(a) (b)

Fig. 2 Modal identification: **a** regular sensor placement ($N=12$), **b** MAC values

and it has values from zero to unity. Figure 2b illustrates the distribution of MAC values of ten reduced natural modes $\Phi_{\mathrm{I}}^{\mathrm{r}}(x)$ of the clamped cylindrical shell-like structure shown in Fig. 2a. The numerically reduced natural modes are extracted from the numerical natural modes Φ_{I} which were obtained by the FE modal analysis using the regular (i.e., uniform) placement of 12 vibration sensors. The orthogonality between the reduced natural modes becomes better as the off-diagonal MAC values tend to zero and the diagonal ones approach unity. There is no doubt that the best case is when MAC has only the diagonal values of unity, which implies that the reduced natural modes are identical with those obtained by the mathematically orthogonal extraction process. In this context, the sensor placement optimization can be sought by minimizing the objective function $F(X)$ defined by

$$F(X) = \sum_{I,J=1,\, I<J}^{n} \mathrm{MAC}_{IJ}(X) \tag{6}$$

which is an arithmetic sum of the off-diagonal MAC values. Here, $X = \left\{ x_1^s,\ x_2^s, \ldots, x_N^s \right\}^T$ denotes the $(2N \times 1)$ design variable vector with $x_{\mathrm{i}} = \left(z_{\mathrm{i}}, \theta_{\mathrm{i}}\right)^{\mathrm{T}}$, and its optimization can be effectively accomplished by employing a genetic algorithm [16, 25].

Meanwhile, the numerical approximation of a damped structural vibration problem using a $m-$ DOF finite element mesh ends up with a linear matrix equation system given by

$$[M]\ddot{\overline{u}} + [C]\dot{\overline{u}} + [K]\overline{u} = F \tag{7}$$

with $\overline{u}$ being the $(m \times 1)$ nodal displacement vector. Substituting the mode superposition $\overline{u}(x;t) = [\Phi(x)]q(t)$ into Eq. (7) and multiplying the $(m \times m)$ matrix $[\Phi]$ of numerical natural modes lead to

$$[\Phi]^{\mathrm{T}}[M][\Phi]\ddot{q} + [\Phi]^{\mathrm{T}}[C][\Phi]\dot{q} + [\Phi]^{\mathrm{T}}[K][\Phi]q = [\Phi]^{\mathrm{T}}F \tag{8}$$

where $\mathbf{q}$ is the $(m \times 1)$ vector of modal participation factors. From the orthonormality between the numerical natural modes, one can obtain the relation between the modal participation factors q_I and the normalized forces $Q_I = \Phi_I^T F$ for the harmonic response: $\left[\left(\omega_I^2 - \omega^2\right) + 2\zeta\omega_I\omega\right]q_I = Q_I$ $(I = 1, 2, \ldots, m)$. In the mode superposition method, the coefficients q_I are determined using the known Q_I and the damping ratio ς, and then the structural vibration field $\overline{u}(x;t)$ is to be obtained [26].

Similarly, in the modal expansion method, the vibration field is expanded with the above-mentioned n reduced natural modes $\Phi_I^r (I = 1, 2, \ldots, n)$. But, the corresponding $(n \times 1)$ modal participation vectors $\mathbf{q}_{n\times 1}$ are to be determined using the nodal responses $\overline{\mathbf{u}}^m$ which were measured at the N sensor positions. Then, by letting $\left\{\Phi_1^{\mathrm{r}}, \Phi_2^{\mathrm{r}}, \cdots, \Phi_{\mathrm{n}}^{\mathrm{r}}\right\}$ be the $(N \times m)$ matrix $[\Phi^{\mathrm{r}}]_{N\times n}$, the relation given by $\overline{\mathbf{u}}_{N\times 1}^m = [\Phi^r]_{N\times n}\mathbf{q}_{n\times 1}$ leads to

$$q_{n\times 1} = [\Phi^r]_{n\times N}^{*}\overline{u}_{N\times 1}^m \tag{9}$$

to determine the modal participation factors q. Here, $[\Phi^{\mathrm{r}}]^* = \left([\Phi^{\mathrm{r}}]^{\mathrm{T}}[\Phi^{\mathrm{r}}]\right)^{-1}[\Phi^{\mathrm{r}}]^{\mathrm{T}}$ denotes the left generalized inverse of the non-square matrix $[\Phi^{\mathrm{r}}]$ [27].

4 Numerical experiments

In this section, the proposed numerical analysis procedure for the structural-acoustic problem is illustrated and the dependence of the numerical results on the sensor placement is investigated. The thin elastic shell-like structure shown in Fig. 2a was taken for the numerical experiments, where the length L, the diameter D and the thickness t are 500, 250 and 20 m, respectively. The structure is manufactured with steel and its material properties are as follows: the density ρ of 7850 kg/m^3, Young's modulus E of 210 GPa and Poisson's ratio ν of 0.3. The shell domain is uniformly discretized by 25×40 in the shell axis and circumferential directions using 4-node shell elements so that the total number of elements is 1,000. The numerical natural modes Φ_{I} are obtained by the finite element modal analysis using a commercial FEM code, MSC/Nastran. According to the detailed numerical results, the lowest natural frequency is $744.60Hz$ and the total number of natural modes that are contained within the frequency range $0 \sim 2500$ Hz is 10 for the cylindrical structure with the clamped-free boundary condition. Likewise, the lowest (flexible) natural frequency is *838.5* Hz and the total number of natural modes that are contained within the frequency range $0 \sim 2500$ Hz is also 10 for the cylindrical structures with the free-free boundary condition. In addition, the lowest natural frequency is *1549.6* Hz, and the total number of natural modes that are contained within the frequency range *0 ~ 2500* Hz is 10 for the cylindrical structure with the clamped–clamped boundary condition. Figure 3 shows the lowest natural modes of the cylindrical shell-like structure for three different boundary conditions.

Figure 4 shows the optimum placement of 12 vibration sensors which was obtained by our GA-based optimization method introduced in our previous paper [16]. It is clearly observed that the optimum sensor placement shown in Fig. 4a is quite different from the regular one shown in Fig. 2a even though both have the same boundary condition. In addition, when compared with Fig. 2b, the MAC values in Fig. 4b of the reduced 10 natural modes $\Phi_{\mathrm{I}}^{\mathrm{r}}$ which were extracted from the numerical modes Φ_{I} using the optimum sensor positions are shown to be much better such that the off-diagonal MAC values are significantly

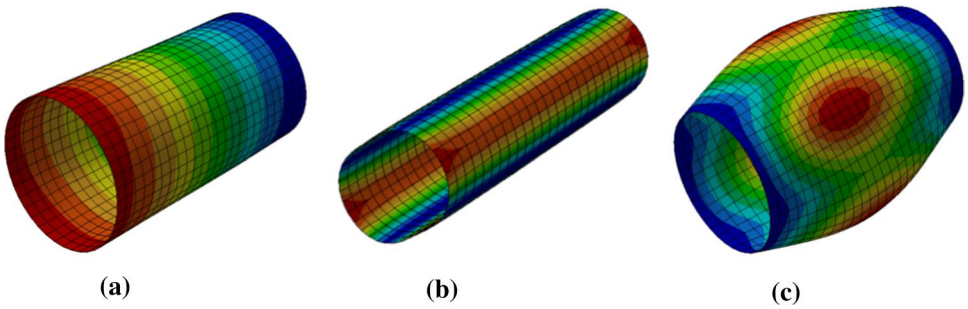

Fig. 3 Lowest (flexible) mode shapes for different boundary conditions: **a** clamped-free, **b** free-free, **c** clamped–clamped

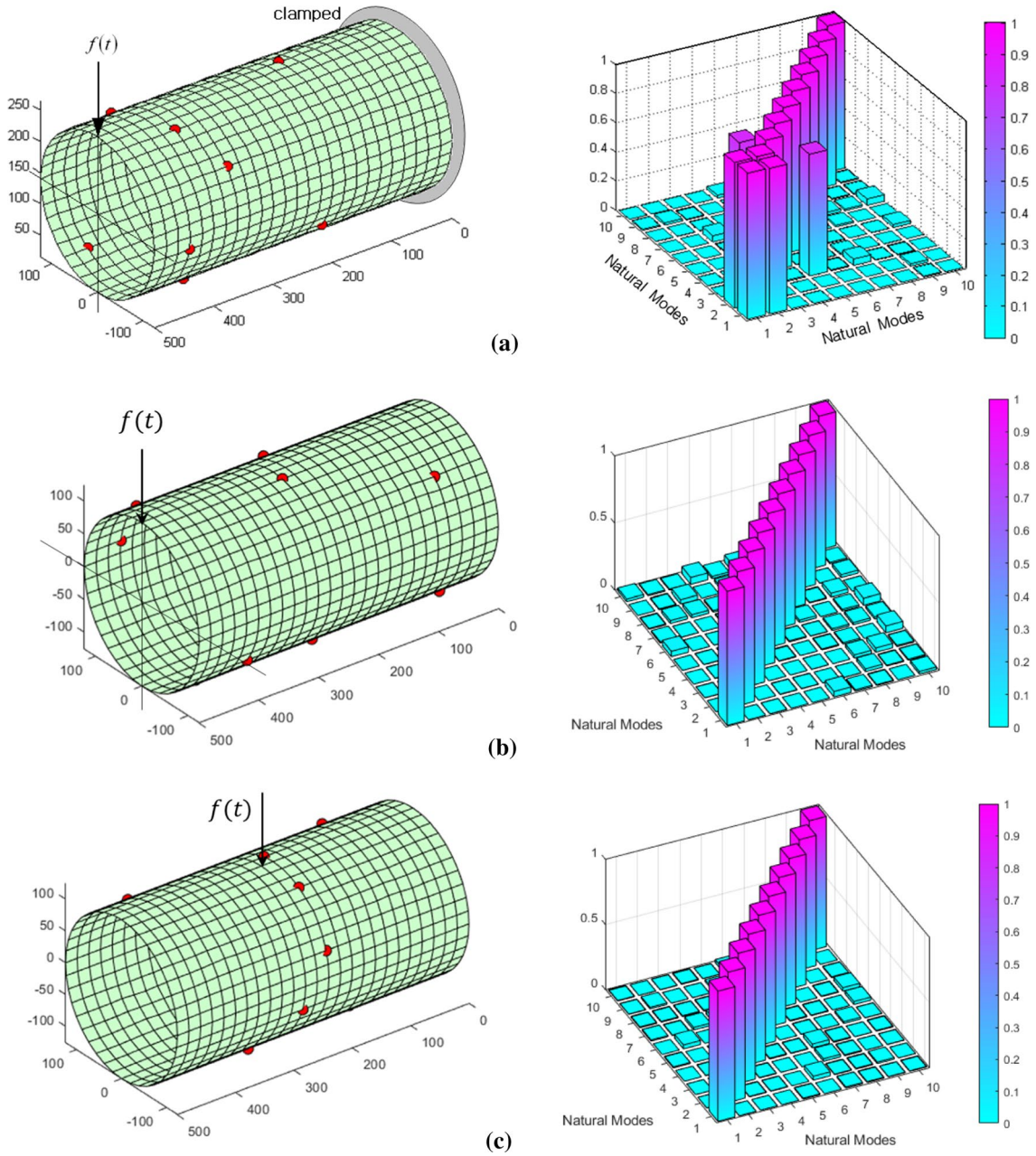

Fig. 4 Optimum sensor placements and MAC values for the cylindrical shell: **a** clamped-free, **b** free-free, **c** clamped–clamped

reduced. Regarding the GA-based sensor placement optimization, the reader may refer to our previous paper for its detailed explanation, rather we here summarize the core parts and the optimization results. The optimum positions $X_{\text{opt}} = \left\{ x_1^s,\ x_1^s, \ldots, x_{12}^s \right\}$ of 12 vibration sensors are sought from all the finite elements nodes, except for the nodes lying on the right clamped boundary. So, each genome in the genome population is defined by the co-ordinates $x_{\text{i}} = \left(z_{\text{i}}, \theta_{\text{i}}\right)^{\text{T}}$ of 12 distinct random finite element nodes, and it is expressed by a binary string which represents the co-ordinates of 12 finite element nodes in the binary number system [15]. The objective function $F(X)$ defined in Eq. (6) was minimized through the iterative genetic evolution, for which the population number and the crossover and mutation ratios were set by 50, 0.6, and 0.01, respectively. The stop criterion for terminating the genetic evolution was defined by the relative change in the maximum fitness value of genomes along the iteration, and it was set by 1.0×10^{-4} and the genetic evolution was terminated in 316 iterations.

4.1 Vibration responses

According to the modal expansion method, the vibration field $u(x;t)$ of the structure due to the impact force $f(t)$, a unit impulse signal which can be represented by *1.0* N for all frequencies, which is applied to the left tip of structure is expanded with the reduced 10 natural modes $\Phi_{\text{I}}^{\text{r}}$ up to 2500 Hz for the clamped-free and free-free systems, *3500* Hz for the clamped–clamped system. The frequency responses of vertical acceleration at the point of excitation are compared in Fig. 5a, b, and c, where the reference indicates the response obtained by the direct frequency response analysis using MSC/Nastran. The modal expansion using the optimal sensor placement produces the responses that deviate from the reference with the maximum relative error of 3.97%, but

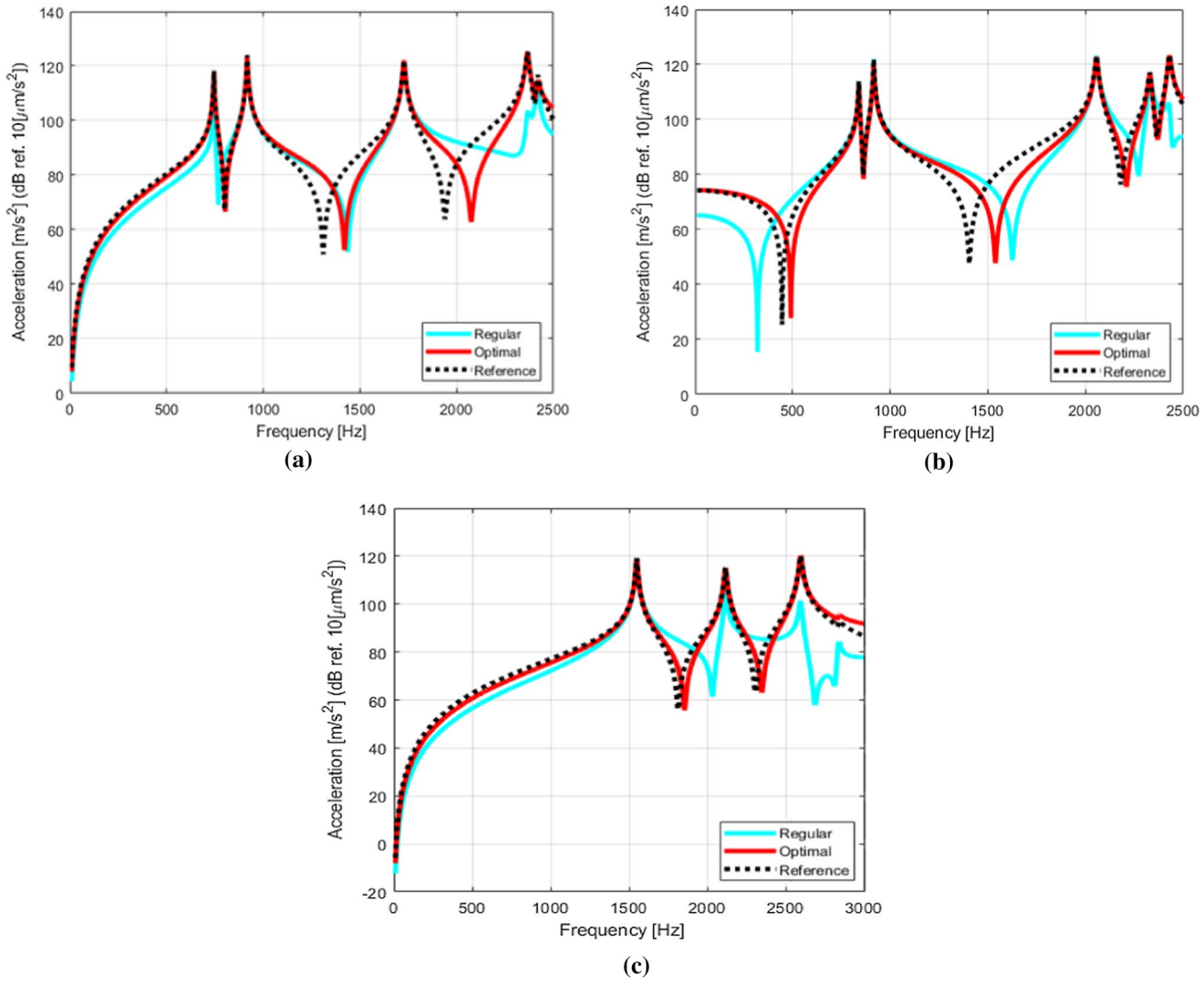

Fig. 5 Frequency responses at the point of excitation: **a** clamped-free, **b** free-free, **c** clamped–clamped

which represents the extraordinary anti-resonances due to the absence of the higher modes in the calculation. Therefore, the responses are in good agreement with the reference except for the anti-resonance frequencies, when compared with the responses obtained using the regular sensor placement showing the maximum relative error of 31.75%. And, the difference between the optimum and regular sensor placements becomes more remarkable as the frequency becomes higher.

The left contours in Figs. 6, 7, 8 represent the vibratory acceleration patterns at the fifth and tenth natural frequencies that were obtained by the direct FE frequency response analysis using MSC/Nastran. Meanwhile, the center and right contours in Figs. 6, 7, 8 show the acceleration patterns reproduced by the modal expansion method using the optimum and regular sensor placements, respectively. It is observed that the optimum sensor placement provides vibratory acceleration patterns that are quite similar to those of MSC/Nastran, but one can see the remarkable difference between the regular sensor placement and MSC/Nastran. In case of the tenth natural frequency, the regular sensor placement leads to a totally different acceleration pattern. It justifies the importance of sensor position such that the modal expansion using the reduced natural modes showing the bad MAC values, as shown in Fig. 2b, leads to the inaccuracy in reproducing the vibration pattern as well as the frequency response. This inaccuracy is also attributed to the inaccurate modal participation factors because the modal participation factors were determined from the reduced natural modes and the measured vibration data.

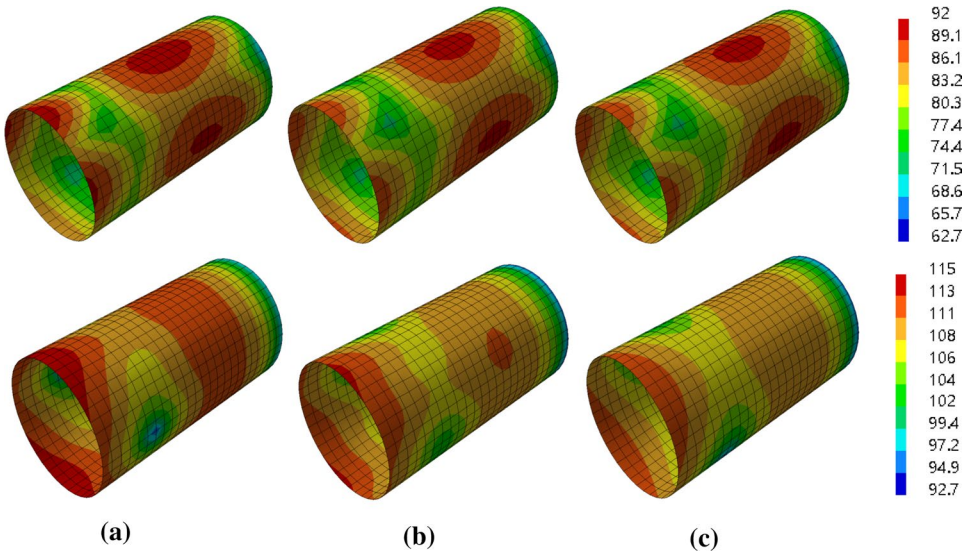

Fig. 6 Vibratory acceleration patterns for the clamped-free cylindrical shell-like structure (*unit:* m/s^2, upper: the fifth natural frequency (1604 Hz), lower: the tenth natural frequency (2418 Hz)): **a** MSC/Nastran, **b** MEM using the optimum sensor placement, **c** MEM using the regular sensor placement

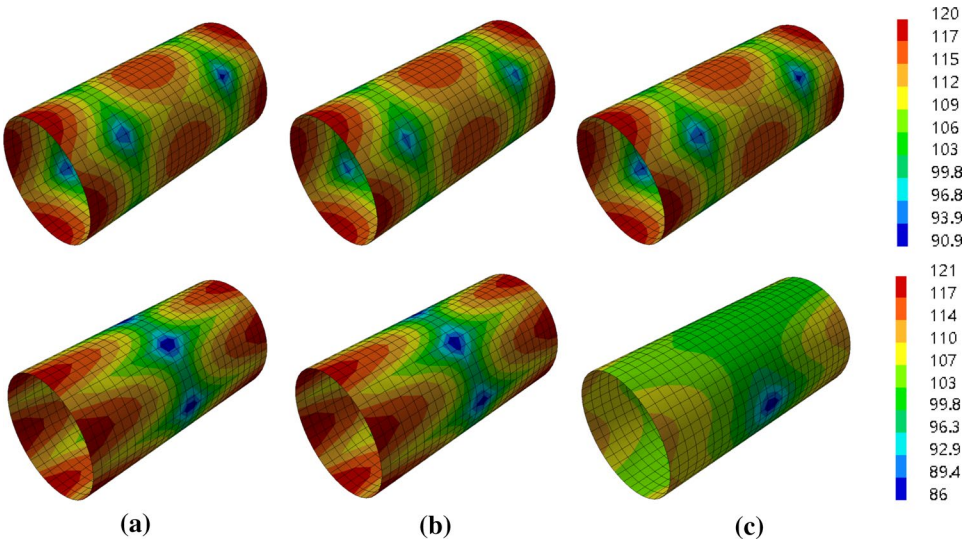

Fig. 7 Vibratory acceleration patterns for the free-free cylindrical shell-like structure (*unit:* m/s^2, upper: the fifth natural frequency (2057 Hz), lower: the tenth natural frequency (2429 Hz)): **a** MSC/Nastran, **b** MEM using the optimum sensor placement, **c** MEM using the regular sensor placement

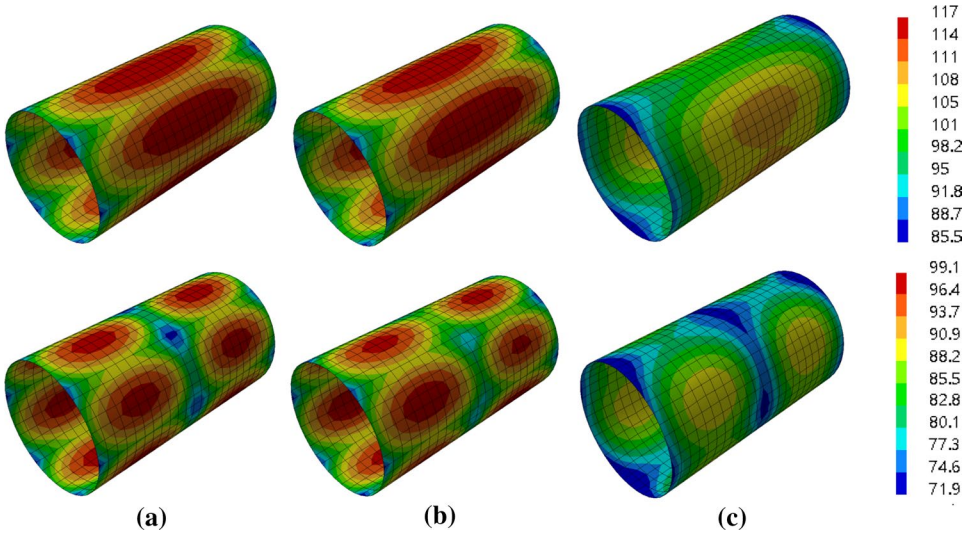

Fig. 8 Vibratory acceleration patterns for the clamped–clamped cylindrical shell-like structure (*unit:* m/s^2, upper: the fifth natural frequency (2597 Hz), lower: the tenth natural frequency (3349 Hz)): **a** MSC/Nastran, **b** MEM using the optimum sensor placement, **c** MEM using the regular sensor placement

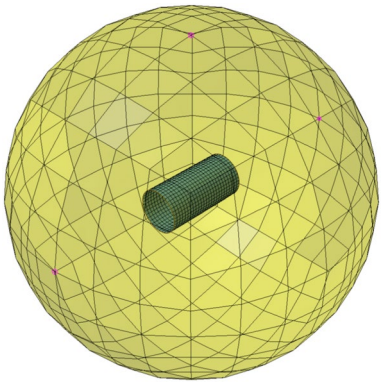

Fig. 9 An acoustic FE model for the acoustic analysis ($R = 1.0$ m)

4.2 Acoustical responses

The vibration field $u(x;t)$ of the cylindrical structure that was reproduced by the modal expansion method is applied to the acoustic analysis. Figure 9 represents an acoustic FE model which was constructed using LMS Virtual. Lab, where the FE mesh of cylinder is the same as for the previous vibration analysis while the field point mesh with the radius R of *1.0* m was generated with 294 volume elements. The perfectly matched layer (PML) technique [23, 28] was employed to prevent the pressure waves from reflecting at the outer surface of the acoustic mesh back to the cylindrical structure. The radiated sound power and pressure were calculated by the acoustic transfer vector (ATV) technique [29, 30] using the modal participation factors of the vibrating cylindrical structure.

The acoustic analysis was carried out with two different structural vibration data that were reproduced by the modal expansion method using the regular and optimum sensor placements. As well, it was also performed by MSC/Nastran for the comparison purpose. The sound pressure patterns at the field point surface for three different boundary conditions are comparatively represented in Figs. 10, 11, 12. At the fifth natural frequency, it is observed that both the regular and optimum sensor placements provide the sound pressure contours that are almost similar to MSC/Nastran. However, the remarkable difference between the regular and optimum sensor placements is observed at the tenth natural frequency. The optimum sensor placement provides sound pressure contour that is in good agreement with MSC/Nastran, but the regular one leads to the sound pressure contour that is remarkably different from MSC/Nastran. It is because the vibration field reproduced using the regular sensor placement is different from one of MSC/Nastran at higher frequencies, as shown in Fig. 5.

The sound power at the field point is comparatively represented in Fig. 13, where the reference stands for the result of MSC/Nastran. The optimum sensor placement shows good agreement with MSC/Nastran with the maximum relative error of 3.13% in a whole range of frequencies, but the regular one shows a remarkable difference with the maximum relative error of 15.67% at the frequencies higher than 1800 Hz. Thus, it has been justified that the structural vibration field which was reproduced using the optimum sensor placement provides the sound power and pressure that are in good agreement with MSC/Nastran in a whole frequency range of interest. The reason why the error in the acoustic response is smaller than the error in the vibration response is that Fig. 13 represents the radiated powers which were obtained by the area integral of intensities (i.e., the product of the sound pressure and the normal velocity) at each point, not the level of radiated noise at a specific point. If the response is observed at a specific sound receiving point, the error would apparently appear at the baseline

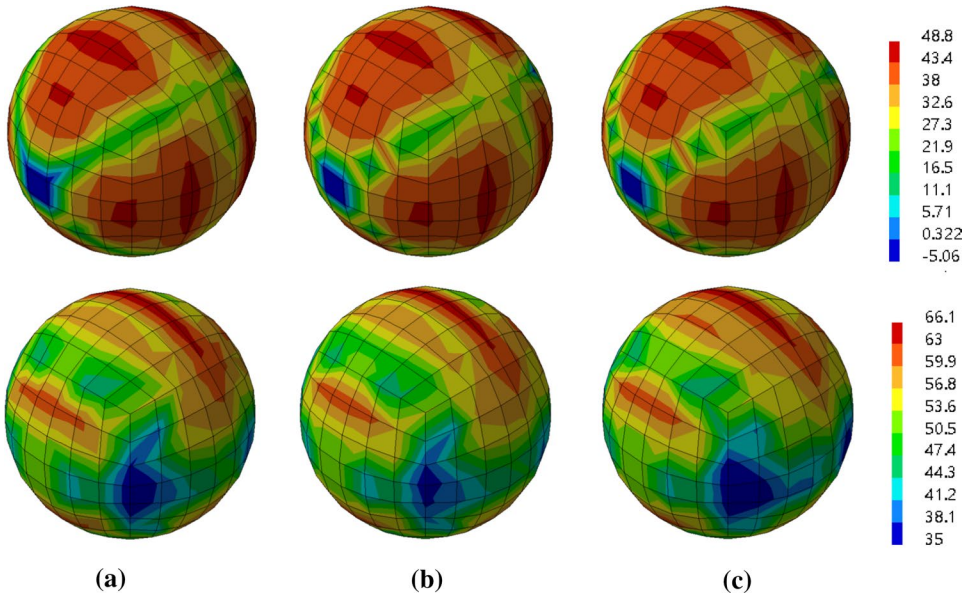

Fig. 10 Sound pressure contours for the clamped-free cylindrical shell-like structure (*unit:* Pa, upper: at the fifth natural frequency 1604 Hz, lower: at the tenth natural frequency 2418 Hz): **a** MSC/Nastran, **b** optimum sensor placement, **c** regular sensor placement

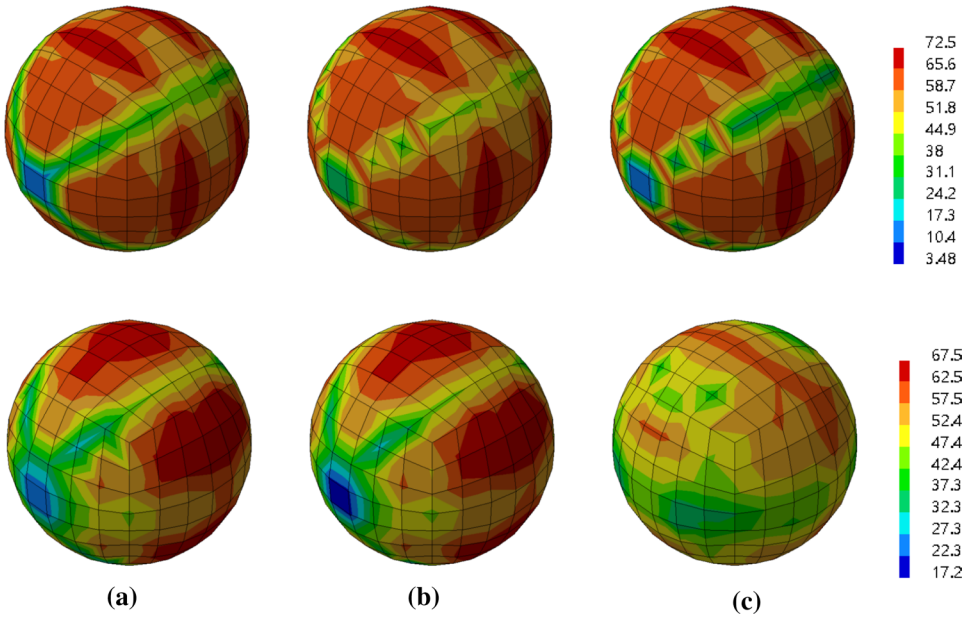

Fig. 11 Sound pressure contours for the free-free cylindrical shell-like structure (*unit*: Pa, upper: at the fifth natural frequency 2057 Hz, lower: at the tenth natural frequency 2429 Hz): **a** MSC/Nastran, **b** optimum sensor placement, **c** regular sensor placement

or at the anti-resonance, like in Figs. 10, 11, 12 and as in the trend of vibration. But, in Fig. 13 representing the radiated power, the point showing the highest intensity gives rise to a dominant effect.

5 Conclusion

A vibroacoustic analysis method by utilizing the modal expansion method and the sensor placement optimization has been introduced in this paper. The vibration field of flexible cylindrical structure subject to the external excitation was reproduced by the modal expansion method, for which the modal participation factors were determined using the vibration data obtained at the optimum sensor positions that were sought with the help of a genetic algorithm. Using the reproduced structural vibration data, the sound patterns, power, and pressure that are resulted from the structural vibration were calculated by the ATV technique. The numerical accuracy of the proposed analysis method was examined by comparing with MSC/Nastran and the case using the regular sensor placement. From the comparative numerical experiments for three different boundary conditions, it has been justified that the proposed method provides the vibration and acoustic responses that are five times better than the case using the regular sensor placement. The case using the regular sensor placement leads

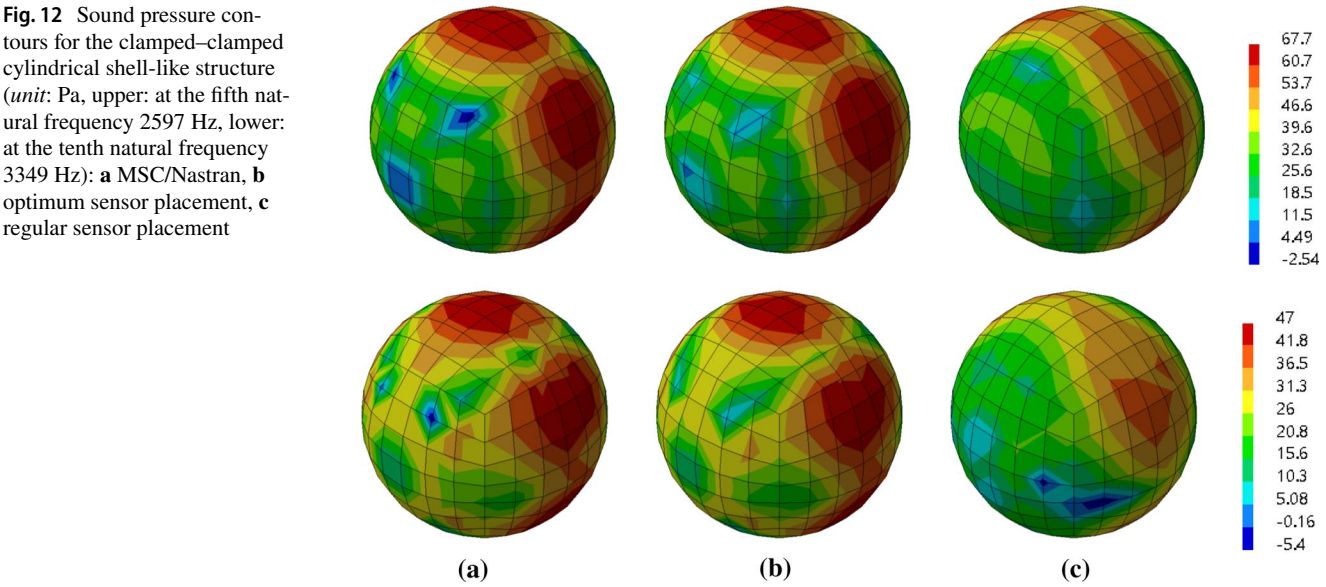

Fig. 12 Sound pressure contours for the clamped–clamped cylindrical shell-like structure (*unit*: Pa, upper: at the fifth natural frequency 2597 Hz, lower: at the tenth natural frequency 3349 Hz): **a** MSC/Nastran, **b** optimum sensor placement, **c** regular sensor placement

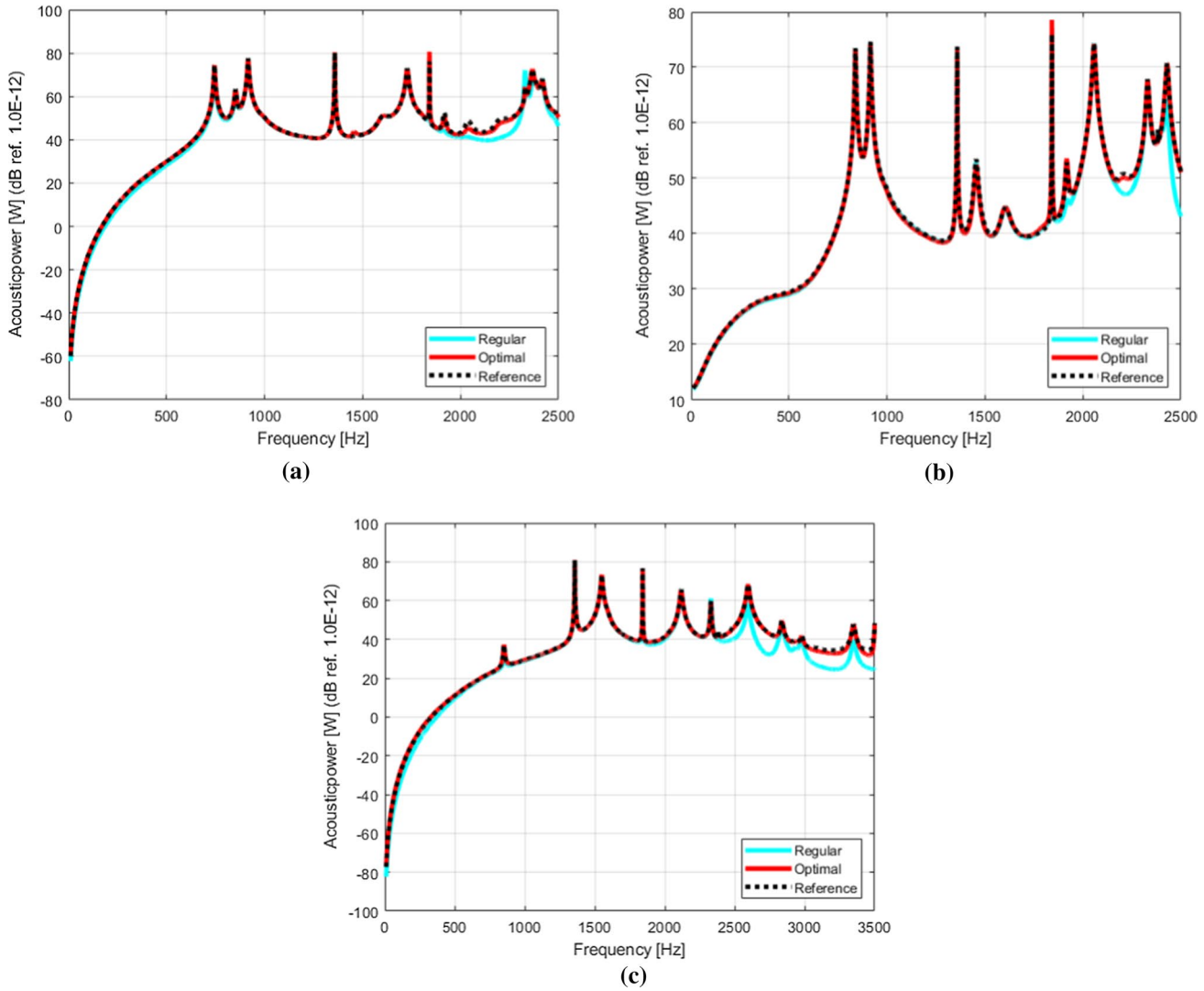

Fig. 13 Comparison of acoustic power results: **a** clamped-free, **b** free-free, **c** clamped–clamped

to remarkably inaccurate results (the maximum relative errors: 31.75% in the vibration response and 15.67% in the acoustical response), in particularly at higher frequencies. But, the case using the optimum sensor placement provides the vibration and acoustic responses that are in good agreement with MSC/Nastran in a whole frequency range of interest (the maximum relative errors: 3.97% in the vibration response and 3.13% in the acoustical response).

References

1. Avsar Y, Gonullu MT (2005) Determination of safe distance between roadway and school buildings to get acceptable school outdoor noise level by using noise barriers. Build Environ 40(9):1255–1260
2. Shur M, Spalart P, Strelets M, Garbaruk A (2006) Further steps in LES-based noise prediction for complex jets. 44th AIAA aerospace sciences meeting and exhibit AIAA: 2006–485
3. Lopes LV, Burley CL (2011) Design of the next generation aircraft noise prediction program: ANOPP2. In: 17th AIAA/CEAS aeroacoustics conference, AIAA: 2011–2854
4. Junger MC, Feit D (1993) Sound, structures, and their interaction. Acoustical Society of America
5. Sandberg GE, Hansson PA, Gustavsson M (2001) Domain decomposition in acoustic and structure-acoustic analysis. Comput Methods Appl Mech Eng 190(24–25):2979–2988
6. Ding WP, Chen HL (2001) A symmetrical finite element model for structure-acoustic coupling analysis of an elastic, thin-walled cavity. J Sound Vib 243(3):547–559
7. Minami S, Kawai H, Yoshimura S (2012) Parallel BDD-based monolithic approach for acoustic fluid-structure interaction. Comput Mech 50(6):707–718
8. Matthies HG, Steindorf J (2002) Partitioned but strongly coupled iteration schemes for nonlinear fluid-structure interaction. Comput Struct 80(27–30):1991–1999
9. Cho JR, Park SW, Kim HS, Rashed S (2008) Hydroelastic analysis of insulation containment of LNG carrier by global-local approach. Int J Numer Methods Engng 76:749–774
10. Brinkmeier M, Nackenhorst U, Peterson S, von Estorff O (2008) A finite element approach for the simulation of tire rolling noise. J Sound Vib 309:20–39
11. Bernard ML, Bronowicki AJ (1994) Modal expansion method for eigensensitivity with repeated roots. AIAA J 32:1500–1506
12. Rao AR, Anandakumar G (2008) Optimal sensor placement techniques for system identification and health monitoring of civil structures. Smart Struct Syst 4(4):465–492
13. Yi TH, Li HN, Gu LM (2012) Sensor placement for structural health monitoring of Canton Tower. Smart Struct Sys 19(4):313–329
14. Stephan C (2012) Sensor placement for modal identification. Mech Syst Signal Process 27:461–470
15. Cho JR, Lee JH, Jeong KM, Kim KW (2012) Optimum design of run-flat tire insert rubber by genetic algorithm. Finite Elem Anal Des 52:60–70
16. Jung BK, Cho JR, Jeong WB (2015) Sensor placement optimization for structural modal identification of flexible structures using genetic algorithm. J Mech Sci Technol 29(7):2775–2783
17. LMS International NV, LMS Virtual.Lab REV9 NVM Standard Training. Belgium
18. Cho JR, Song JM (2001) Assessment of classical numerical models for the separate fluid-structure modal analysis. J Sound Vib 239(5):995–1012
19. Xing JT (2007) Natural vibration of two-dimensional slender structure-water interaction systems subject to Sommerfeld radiation condition. J Sound Vib 308:67–79
20. Keller JB, Givoli D (1989) Exact non-reflecting boundary conditions. J Comput Phys 82(1):172–192
21. Wrobel LC (2002) The boundary element method, applications in thermo-fluids and acoustics. John Wiley & Sons, New York
22. Astley RJ (2000) Infinite element formulations for wave problems: a review of current formulations and an assessment of accuracy. Int J Numer Methods Eng 49:951–976
23. Kim MS, Jeon SH, Cho JR, Jeong WB (2014) Comparative evaluation of PML technique for hydrodynamic impact loading on spar-type floating platform. Ocean Eng 85:80–92
24. Allemang RJ, Brown DL (1982) A correlation coefficients for modal vector analysis. In: Proc int modal anal conference, pp 110–116
25. Liu W, Gao WC, Sun Y, Xu MJ (2008) Optimal sensor placement for spatial lattice structure based on genetic algorithms. J Sound Vib 317:175–189
26. Cho JR, Song JM, Lee JK (2001) Finite element techniques for the free-vibration and seismic analysis of liquid-storage tanks. Finite Elem Anal Des 37:467–483
27. Li FL, Hu XY, Zhang L (2013) Left and right inverse eigenpairs problem for -Hermitian matrices. J Appl Math ID 230408:1–6
28. Berenger JP (1994) A perfectly matched layer for the absorption of electromagnetic waves. J Comput Phys 114(2):185–200
29. Tournour M, Dessart S, McCulloch C (2002) On the accuracy of vibrao-acoustic solutions using the atv method. In: Pro ISMA 2002, Leuven, Belgium
30. von Estorff O (2003) Efforts to reduce computation time in numerical acoustics an overview. Acta Acust Acust 89(1):1–13